

Exact-diagonalization studies of trion energy spectra in high magnetic fields

Arkadiusz Wójs,^{1,2} and John J. Quinn²

¹*Institute of Physics, Wrocław University of Technology, Wybrzeże Wyspiańskiego 27, 50-370 Wrocław, Poland*

²*Department of Physics, University of Tennessee, Knoxville, TN 37996, USA*

Binding energies of negative and positive trions in doped GaAs quantum wells in high magnetic fields are studied by exact numerical diagonalization in spherical geometry. Compared to earlier calculations, finite width of the quantum well and its asymmetry caused by one-sided doping are both fully taken into account by using self-consistent subband wave functions in the integration of Coulomb matrix elements, and by inclusion of higher subbands along with several Landau levels in the Hilbert space. Detailed analysis of the accuracy and convergence of the exact diagonalization scheme is presented, including dependence on Landau level and subband mixing, sensitivity to the (not well known) single-particle spectrum in the valence band, and the estimate of finite-size errors. The main results are the exciton dispersion and trion binding energy spectrum calculated as a function of the magnetic field, quantum well width, electron concentration, and the presence of an ionized impurity. As a complementary approach, a combination of the exact diagonalization in the quantum well plane and the variational calculation in the normal direction is used as well.

PACS numbers: 71.35.Pq, 71.35.Ji, 71.10.Pm

I. INTRODUCTION

Photoluminescence (PL) is a powerful method in the experimental studies of two-dimensional (2D) electron systems in high magnetic fields.^{1,2,3} In a typical experiment, an additional electron-hole (e - h) pair is introduced into the electron system through absorption of a photon. This causes energy relaxation via Coulomb scattering, followed by optical recombination of the well-defined, quantized eigenstates involving an e - h pair coupled in different ways to the surrounding electrons.

This coupling is a response of the 2D electron system to the perturbation associated with the photo-injection of a hole (particle of the opposite charge). Depending on the nature of this response and on the number of electrons involved, the PL spectrum either reveals information about dynamics of an illuminated system⁴ or “merely” probes the few-body excitonic complexes which form under given conditions (quantum well geometry, magnetic field, etc.) but are weakly affected by the surrounding electrons.

The latter scenario occurs at sufficiently high magnetic fields B and low electron concentrations ρ , corresponding to small Landau level (LL) filling factors $\nu = 2\pi\rho\lambda^2$ (with $\lambda = \sqrt{\hbar c/eB}$ being the magnetic length). The PL spectra at $\nu \ll 1$ are usually dominated by recombination of three-body states called trions ($X^- = 2e + h$), consisting of an exciton ($X = e + h$) bound to an additional electron.^{5,6} The trion binding energy is

$$\Delta = E_X - E_{X^-}, \quad (1)$$

where E is the X/X^- ground state energy. The lowest LL energy ε_0 is set to zero for each particle.

The exhaustive reviews of experimental and theoretical work on trions have been written by Peeters *et al.*,⁷ Bar-Joseph,⁸ and also by us.⁹ Let us hence only summarize here that despite involving only three particles, quantum dynamics of a trion in the presence of confinement

and magnetic field is neither trivial nor completely understood. The complications include the competition of several (cyclotron, Coulomb, subband, and Zeeman) energy scales, complex structure of the valence band, spin-orbit effects (and their effect on relaxation), and coupling to free carriers, lattice defects, and phonons.

However, it is established that, depending on the parameters (composition and width w of the quantum well, electron concentration ρ , magnetic field B , etc.), the trion energy spectrum contains one or more bound states, distinguished by the total spin of the pair of electrons S and the relative angular momentum \mathcal{M} . (i) At small B , the only bound trion is the “singlet” X_s^- with $S = 0$ and $\mathcal{M} = 0$, a 2D analog of the Hydrogen ion.^{5,10} It was first observed in CdTe by Kheng *et al.*⁶ and then also in GaAs^{11,12,13,14} and ZnSe^{15,16} (with considerably different effective Rydbergs Ry and Bohr radii a_B). Positive singlet trions $X^+ = 2h + e$ (with the opposite effective-mass ratio) were also observed^{17,18} in acceptor-doped samples. (ii) In the (unrealistic) limit of very high B and vanishing w , the singlet trion unbinds as predicted from the “hidden symmetry”^{19,20,21} (particle-hole symmetry between conduction electrons and valence holes in the lowest LL). However, it is replaced by a different bound state: the “dark triplet” X_{td}^- with $S = 1$ and $\mathcal{M} = -1$,²² and with an infinite optical lifetime.^{23,24} Despite initial difficulties²⁵ it was also eventually detected in PL,^{26,27,28} and its vanishing oscillator strength was confirmed directly in optical absorption.²⁹ The singlet-triplet crossover occurs in rather high magnetic fields,³⁰ and it is fairly sensitive to the parameters.^{31,32,33} (iii) Additional, less strongly bound trions occur at intermediate fields, including the “bright triplet” X_{tb}^- with $S = 1$ and $\mathcal{M} = 0$.³¹ All three trions were later confirmed by several independent calculations^{32,34} and experiments.^{27,28,35,36}

Trions were also identified beyond the “dilute regime,” in PL spectra of the fractional quantum Hall states. It was found³⁷ that a trion immersed in a Laughlin $\nu = 1/3$

liquid may survive in form of a fractionally charged “quasiexciton” state which retains the characteristic internal e - h correlations of its trion parent. This extends the variety of systems in which trions occur and also allows to use their recombination spectrum as an indirect probe of incompressible electron fluids.^{38,39} This possibility seems especially attractive for systems in which these fluids may form but cannot be studied by transport.⁴⁰ Remarkably, the recombination spectra of the quasiexcitons formed from different trions and interacting with fractionally charged quasiparticles of the Laughlin liquid behave differently when the filling factor passes through $\nu = 1/3$: they show a discontinuity for the X_{td}^- but no anomaly for the X_s^- . Therefore, the quantum wells for studying incompressible fluids by PL need be designed so as to yield the X_{td}^- ground state. This could be greatly helped by accurate theoretical predictions.

In this paper we address this problem by extensive realistic numerical calculations of the binding energies of (negative and positive) trions in doped GaAs quantum wells in high magnetic fields. Compared to the earlier studies,^{30,31,32,33,34} asymmetry of the quantum well caused by one-sided doping is fully taken into account by self-consistent calculation of the subband wave functions and by inclusion of up to three subbands along with several Landau levels in the Hilbert space. Especially for the singlet trion and for doped wells, the results are significantly different from the previous, less accurate models.

Another goal of this paper is to explain and justify the configuration-interaction exact numerical diagonalization in Haldane spherical geometry for the realistic calculations of the few-body excitonic complexes. The method was recently used in several related studies without giving a detailed description,^{37,41} leaving the questions of its validity and accuracy largely unanswered. The detailed Secs. II and III fill this gap, and with the future studies in perspective, point out the advantages over the (complementary) variational approach.

II. MODEL

A. Haldane spherical geometry

In Haldane’s spherical geometry,⁴² the particles (electrons or holes) are confined to the surface of a sphere of radius R . The radial (i.e., normal to the surface) magnetic field B is produced by a Dirac monopole placed at its center. The monopole strength $2Q = 4\pi R^2 B / \phi_0$ is defined in the units of the $\phi_0 = hc/e$ quantum as the total flux through the surface. This definition can also be rewritten as $R^2 = Q\lambda^2$ which makes clear that Q measures the surface curvature in the units of magnetic length $\lambda = \sqrt{hc/eB}$ (rather than defining a specific B). Also, due to Dirac’s condition, $2Q$ must be integral.

The single-particle states $Y_{Q,l,m}$ form degenerate shells of the eigenstates of angular momentum length l and pro-

jection m . They are called “monopole harmonics.”⁴³ The n th shell has $l = Q + n$ and it corresponds to the n th Landau level (LL). Its degeneracy is $g = 2l + 1$ (m going from $-l$ to l), which scales linearly with B and R^2 .

In the lowest LL ($n = 0$), the $m = \pm Q$ states describe the closest orbits around the opposite poles, while, in general, $\langle z \rangle \propto m$. The wave functions scale with λ . In the $\lambda/R \rightarrow 0$ limit, the sequence of orbitals with $m = Q, Q - 1, Q - 2, \dots$, evolve continuously into the series of states with angular momenta $\mu = 0, -1, -2, \dots$, obtained in the symmetric gauge on a plane. Therefore, also the spherical orbitals with $m = Q + \mu$ can be denoted by the value of μ (both in the lowest the excited LLs).

The spherical geometry was originally proposed for numerical studies of extended systems (such as incompressible quantum liquids). Like confinement or periodic boundary conditions, it allows for having a finite number of electrons (as required for the exact numerical diagonalization of the hamiltonian) in a finite area (to achieve a finite density of the actual, infinite system). However, Haldane’s geometry does it without breaking the 2D translational symmetry, essential for various properties of the liquid. The 2D rotational symmetry of the sphere replaces the symmetry of the plane and leads to the conservation of (the same number of) two orbital quantum numbers – two components of the total angular momentum: length L and projection L_z .

Due to the relation between orbital Hilbert eigenspaces in both geometries, the “spherical” L and L_z correspond to the “planar” quantum numbers. The *neutral* excitations, which on a plane move along straight lines with well defined wave vectors k , on a sphere move along great circles and carry a conserved $L = kR$ (the degeneracy associated with L_z corresponds to that of the orientation of the wave vector, and the quantization of L and L_z is a finite size effect). The *charged* excitations move along the (quantized) cyclotron orbits in both geometries, and L must be interpreted in terms of the planar angular momentum M rather than in terms of k (in this case, finite-size affects the orbit by the surface curvature only). Clearly, for the spherical geometry to be useful, the characteristic length of correlations responsible for the studied effect must scale with λ , so that it can be made smaller than R (and the finite size effects can be eliminated by the $2Q \rightarrow \infty$ extrapolation).

Haldane’s geometry has also become useful in studying excitons or trions. The sole advantage is the 2D rotational symmetry of the sphere, preserving the degeneracy of the trion LLs in a finite size calculation. The decoupling of trion’s relative dynamics from the cyclotron motion of its “center of mass” (CM) is a big help in the identification of different trions in the energy spectra, especially of the less strongly bound states. We put CM in parentheses here, since it is not exactly the CM motion that decouples for charged complexes in a magnetic field.

Different trion states are distinguished by their relative (spin and orbital) correlations, reflected in difference in the relative angular momentum \mathcal{M} . The CM excitations

carry an arbitrary (negative) angular momentum \mathcal{M}_{cm} and lead to each trion having its own LL accommodating different total angular momenta $M = \mathcal{M} + \mathcal{M}_{\text{cm}}$. Let us stress that the proper definition of \mathcal{M} and \mathcal{M}_{cm} independently conserved in the magnetic field is non-trivial by involving the “magnetic translation” generators.^{24,46}

If, in order to facilitate numerical diagonalization, the single-particle basis is restricted to several lowest single-particle orbitals: $|\mu| \leq \mu_{\text{max}}$, then \mathcal{M}_{cm} and \mathcal{M} are no longer independently conserved. This causes artificial dependence of computed trion energies on M and makes distinction of different trions more difficult. This problem does not occur in spherical geometry, in which the trion LLs have a form of angular momentum multiplets with $L = Q + \mathcal{M}$. Resolving L (a conserved number regardless of finite LL degeneracy) in the diagonalization makes the identification simple: each bound L -multiplet is a genuine trion state. Exact diagonalization in either geometry may be combined with the size extrapolation to eliminate finite-size (qualitative and quantitative) errors.

Let us summarize the differences of both approaches. On the plane, the Coulomb matrix elements are accurate at each value of μ_{max} , but the trion LL degeneracies are only restored in the $\mu_{\text{max}} \rightarrow \infty$ limit. On the sphere, the 2D symmetry holds at each $2Q$, but the interaction matrix elements depend on surface curvature. The last effect can be reduced by calculation of matrix elements from Haldane pseudopotentials for a plane (using the spherical expansion and Clebsch-Gordan coefficients), helpful when the $2Q \rightarrow \infty$ extrapolation is impossible.

B. Hamiltonian matrix elements

1. Basis

For diagonalization of the hamiltonian H we choose the configuration interaction (CI) basis, e.g.,

$$|i, j; k\rangle = c_i^\dagger c_j^\dagger d_k^\dagger |\text{vac}\rangle \quad (2)$$

for the trion. Here c^\dagger and d^\dagger are electron and hole creation operators, and the composite indices i, j , and k include all relevant single-particle quantum numbers (spin σ , well subband s , LL index n , and angular momentum m). Although for only two or three particles the CI basis does not produce as sparse matrices of the (two-body) hamiltonian as for many-electron systems, it is still a convenient choice for the evaluation of matrix elements. The single-particle states used in the exciton and trion basis include both spin projections ($\sigma = \uparrow$ and \downarrow), up to five lowest LLs ($n \leq 4$) and three lowest subbands ($s \leq 2$) for electrons and holes. Different values of $2Q \leq 30$ were used to eliminate dependence on finite LL degeneracy.

The pair electron spin S (for the trion) and total angular momentum L as well as their projections $S_z = \sum \sigma$ and $L_z = \sum m$ are all conserved quantum numbers. The CI basis is the eigenbasis of S_z and L_z , while the energy

(excluding the Zeeman term) only depends on S and L . Therefore, only the subspace corresponding to the minimum values of $S_z = 0$ and $L_z = 0$ (or $1/2$, if half-integral) need be diagonalized, containing all S and L states and thus covering the entire energy spectrum.

2. One-body terms

The exact cyclotron energy on the sphere is

$$\varepsilon_n = \hbar\omega_c \left(n + \frac{1}{2} + \frac{n(n+1)}{2Q} \right). \quad (3)$$

In calculation, the last term equal to $n(n+1)\hbar^2/2J$ (here, $J = m^*R^2$ is the moment of inertia on a sphere, and m^* is the effective mass, not to be confused with angular momentum) was omitted as a finite-size artifact, and the realistic values of $\hbar\omega_c$ for GaAs were taken from experiment. For electrons, $\hbar\omega_c/B = 1.78$ meV/T; for the heavy holes we used the following interpolated formula

$$\hbar\omega_c = \alpha(1 + \beta_1 w^{-2}) + \gamma(1 + \beta_2 w^{-2})B, \quad (4)$$

with the following parameter set: $\alpha = 0.45$ meV, $\gamma = 0.282$ meV/T, $\beta_1 = 275$ meV nm² and $\beta_2 = 10$ meV nm², taken after Cole *et al.*⁴⁷ and expected to work adequately at $B \geq 10$ T in $w = 10 - 30$ nm wells (in doped wells, the actual effective width of the hole layer is used for w).

Although Eq. (4) describes well only the $n = 0 \rightarrow 1$ gap, we used it (for the lack of better information) to model scattering to higher LLs as well, and tested sensitivity to this approximation. We also neglected the mixing of heavy and light holes (off-diagonal terms of the Luttinger-Kohn hamiltonian). We expect these approximations to affect the negative trion binding energy Δ much less than each of the exciton and trion energies, E_X and E_{X-} , separately. However, a more accurate treatment of the hole LL spectrum might considerably improve the model for the positive trions.

The energies of higher quantum well subbands (excited states in the z -direction) \mathcal{E}_s were calculated as a function of well width w and electron concentration in the well ϱ . In doped wells ($\varrho > 0$), the electric field of the remote ionized donors penetrates the quantum well, affecting the positions of occupied energy levels in the well (for our parameters, it is only \mathcal{E}_0) with respect to the Fermi energy. This in turn affects ϱ and the sheet concentration of ionized donors, and thus also the electric field itself. The Schrödinger and Poisson equations must be therefore solved self-consistently to give the values of \mathcal{E}_s .⁴⁸

As an example, let us look at the values for the $s = 1$ subband (we set $\mathcal{E}_0 = 0$), which for $w = 10 - 30$ nm can be fitted by power-law curves $\mathcal{E}_1 = \zeta w^{-\kappa}$. For the electrons we obtain $\zeta = 3600$ and $\kappa = 1.60$, weakly dependent on doping, and for the holes, $\zeta = 1400$ and $\kappa = 1.87$ for a symmetric well and $\zeta = 430$ and $\kappa = 1.25$ for $\varrho = 2 \cdot 10^{11}$ cm⁻² (the values appropriate for \mathcal{E} measured in meV and w measured in nm). Clearly, strong

subband mixing can be anticipated at least in higher fields and in wider wells (e.g., compare $\mathcal{E}_1 = 30.5$ and 6.9 meV to $\hbar\omega_c = 44.5$ and 7.6 meV for electron and hole, respectively, in a symmetric 20 nm well at $B = 25$ T).

Since the projection of pair electron spin, S_z , is conserved by the Coulomb interaction, the Zeeman energy E_Z does not have to be included in the diagonalization. Instead, the entire energy spectra obtained from the diagonalization without E_Z must be at the end rigidly shifted by $S_z E_Z$. For the trion binding energies it means subtracting one electronic E_Z from Δ of the singlet states (as needed to flip the spin of one of its two unpolarized electrons). In this approximation, the spin-orbit coupling is neglected and it is assumed that that electron and hole E_Z 's are both constants. In fact, they depend on n and s , through Rashba and (in asymmetric structures) Dresselhaus couplings, both mixed by Coulomb interaction.⁴⁹

In the recombination spectrum of excitons or trions, the sum of electron and hole Zeeman energies splits the “ ± 1 ” peaks corresponding to two circular polarizations of light (both present if both electron and hole spins are populated). If E_Z were constant, the same splitting would result for the X and all X^- states. The observed difference^{18,50} reveals the inaccuracy of this approximation. It also reflects different LL and subband mixing in each of these complexes. In our model, the spin-orbit effects can be included as the zeroth order perturbation, given n - and s -dependence of E_Z (the LL and subband occupation numbers are easily extracted from the X and X^- wave functions obtained from the diagonalization).

3. Two-body terms

a. Ideal 2D layers. Let us begin with derivation of the matrix elements of the Coulomb interaction $V_{ee} \equiv V$,

$$V(r) = \frac{e^2}{\epsilon r} \quad (5)$$

(with ϵ being the dielectric constant) for the layers with zero width. We use rays in spherical coordinates $\Omega = (\theta, \phi)$ as the arguments of monopole harmonics and write

$$\begin{aligned} & \langle \sigma'_1, n'_1, m'_1; \sigma'_2, n'_2, m'_2 | V | \sigma_1, n_1, m_1; \sigma_2, n_2, m_2 \rangle \\ &= \delta_{\sigma'_1 \sigma_1} \delta_{\sigma'_2 \sigma_2} \int d^2\Omega_1 d^2\Omega_2 Y_{Q, l'_1, m'_1}^*(\Omega_1) Y_{Q, l'_2, m'_2}^*(\Omega_2) \\ & \quad \times V(r) Y_{Q, l_1, m_1}(\Omega_1) Y_{Q, l_2, m_2}(\Omega_2). \end{aligned} \quad (6)$$

This four-dimensional integral is solved by using the rotation relations for monopole harmonics,⁴⁴

$$\hat{D} Y_{Q, l, m}(\Omega) = e^{i\psi} \sum_{\eta} \mathcal{D}_{\eta, m}^l Y_{Q, l, \eta}(\Omega), \quad (7)$$

different from those for standard spherical harmonics only by an inconsequential phase factor $\psi(Q)$. The Euler rotation⁴⁵ $\hat{D}(0, -\theta_1, -\phi_1)$ moves Ω_1 to the north pole of the sphere \hat{N} . Its Wigner function is

$$\mathcal{D}_{\eta, m}^l \equiv \mathcal{D}_{\eta, m}^l(0, -\theta_1, -\phi_1) = e^{im\phi_1} d_{\eta, m}^l(-\theta_1), \quad (8)$$

where we use standard notation for the reduced function

$$d_{\eta, m}^l(-\theta_1) = (-1)^p \sum_{\tau} \xi_{\eta, m}^{l, \tau} u_1^{2l} (v_1/u_1)^{2\tau+p} \quad (9)$$

with $u_1 = \cos(\theta_1/2)$, $v_1 = \sin(\theta_1/2)$, $p = \eta - m$,

$$\xi_{\eta, m}^{l, \tau} = (-1)^{\tau+p} \sqrt{\binom{l+\eta}{\tau+p} \binom{l-\eta}{\tau} \binom{l+m}{\tau} \binom{l-m}{\tau+p}}, \quad (10)$$

and the summation going over all τ for which none of the arguments of the factorials in ξ are negative.

In Eq. (5), we take the chord distance $r = (\Omega_1 - \Omega_2)R$. From now on, let us use $\theta \equiv \theta_{12}$ for the angle between Ω_1 and Ω_2 . The Coulomb potential becomes

$$V(\theta) = \frac{e^2}{2\epsilon R v}. \quad (11)$$

By applying rotation \mathcal{D} under the integral over Ω_1 we get

$$\begin{aligned} & \langle n'_1, m'_1; n'_2, m'_2 | v^{-1} | n_1, m_1; n_2, m_2 \rangle \\ &= \sum_{\eta} \langle n'_1, m'_1 | \mathcal{D}_{\eta, m'_2}^{l'_2*} \mathcal{D}_{\eta, m_2}^{l_2} | n_1, m_1 \rangle \langle n'_2, \eta | v^{-1} | n_2, \eta \rangle. \end{aligned} \quad (12)$$

Using Eqs. (8–10), the first matrix element above is

$$\begin{aligned} & \langle n'_1, m'_1 | \mathcal{D}_{\eta, m'_2}^{l'_2*} \mathcal{D}_{\eta, m_2}^{l_2} | n_1, m_1 \rangle \\ &= \delta_{m'_1+m'_2}^{m_1+m_2} \sum_{\alpha', \alpha} \xi_{\eta, m'_2}^{l'_2, \alpha'} \xi_{\eta, m_2}^{l_2, \alpha} \mathcal{I}_{n'_1, m'_1}^{n_1, m_1}(a, b) \end{aligned} \quad (13)$$

with $b = 2(\alpha' + \alpha + \eta) - m'_2 - m_2$, $a = 2(l'_2 + l_2) - b$, and

$$\mathcal{I}_{n, m}^{n', m'}(a, b) = 2\pi \int d\cos\theta Y_{Q, l', m'}(\theta) u^a v^b Y_{Q, l, m}(\theta). \quad (14)$$

The second integral in Eq. (12) is, up to a prefactor, an effective one-body Coulomb pseudopotential

$$\mathcal{V}_n^{n'}(m) \equiv \langle n', m | V(\theta) | n, m \rangle \quad (15)$$

describing scattering of an electron or a hole by a point charge (e.g., ionized impurity) located at the north pole. Note that it is different from the definition of Haldane (pair) pseudopotential. The $\mathcal{V}(m)$ for the sphere can be converted into $\mathcal{V}(\mu)$ for the plane via $\mu = m - Q$. This interaction conserves m , but allows for an inter-LL transition $n \rightarrow n'$. Using the symbol I it simply reads

$$\langle n'_2, \eta | v^{-1} | n_2, \eta \rangle = \mathcal{I}_{n'_2, \eta}^{n_2, \eta}(0, -1). \quad (16)$$

To calculate the integral I of Eq. (14) let us recall that

$$Y_{Q, l, m}(\theta) = N_{Q, l, m} u^{Q+m} v^{Q-m} P_n^{Q-m, Q+m}(\cos\theta), \quad (17)$$

where

$$N_{Q, l, m}^2 = \frac{2l+1}{4\pi} \binom{2l}{l+m} \binom{2l}{l+Q}^{-1}, \quad (18)$$

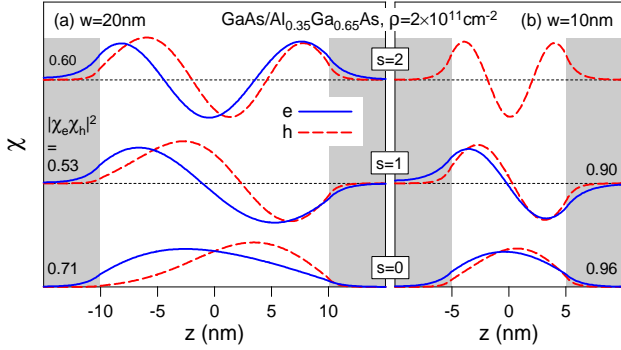


FIG. 1: (color online) Lowest electron and hole subband wave functions $\chi_s(z)$ in GaAs quantum wells of width $w = 10$ nm (a) and 20 nm (b) doped on one side to electron concentration $\rho = 2 \cdot 10^{11} \text{ cm}^{-2}$. Squared electron-hole overlaps are indicated. Note only two bound electron subbands in (b).

and the Jacobi polynomial P can be expanded as

$$P_n^{\alpha, \beta}(x) = \sum_q c_{n,q}^{\alpha, \beta} u^{2(n-q)} v^{2q}, \quad (19)$$

with the coefficients

$$c_{n,q}^{\alpha, \beta} = (-1)^q \binom{n+\alpha}{n-q} \binom{n+\beta}{q}, \quad (20)$$

and the summation range defined by the above factorials.

Finally, substitution of Eqs. (17–20) into Eq. (14) gives

$$I_{n_2, m_2}^{n_1, m_1}(a, b) = N_{Q, l_1, m_1} N_{Q, l_2, m_2} \times \sum_{q_1, q_2} c_{n_1, q_1}^{Q-m_1, Q+m_1} c_{n_2, q_2}^{Q-m_2, Q+m_2} N_{\tilde{Q}, Q, \tilde{m}}^{-2}, \quad (21)$$

where $\tilde{Q} = Q + a + b + (n_1 + n_2)/2$ and $\tilde{m} = a - b + (m_1 + m_2 + n_1 + n_2 - q_1 - q_2)/2$.

By collecting all above equations, a closed expression for the e - e matrix element in a layer of zero width is finally obtained. The e - h elements are found by particle-hole conjugation (with i below being composite indices)

$$\langle i'_1; i'_2 | V_{eh} | i_1; i_2 \rangle = - \langle i'_1; i_2 | V_{ee} | i_1; i'_2 \rangle. \quad (22)$$

b. Layers of finite width. In the ideal 2D limit, the interaction matrix V depended on B only through the overall scale e^2/λ . A finite width w of the quantum well, causing finite extent of wave functions in the normal (z) direction, introduces an additional parameter $w/\lambda \propto \sqrt{B}$ that affects matrix elements individually. This is true even in the simplest case when the quantum well asymmetry and the difference between electron and hole subband wave functions can be neglected. Hence, the matrix elements no longer explicitly depend only on $2Q$ (surface curvature), but also on the form of subband wave functions and on B (via the w/λ length scale ratio).

The realistic electron and hole subband wave functions $\chi_s(z)$ for asymmetrically doped quantum wells were calculated self-consistently⁴⁸ (together with the subband energies \mathcal{E}_s of Sec. II B 2). An example is shown in Fig. 1

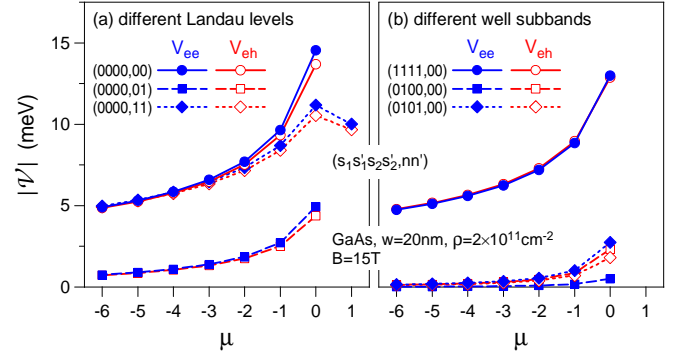


FIG. 2: (color online) Examples of one-body pseudopotentials (interaction energy \mathcal{V} vs angular momentum μ) defined by Eq. (24) and used in calculation of two-body matrix elements for e - e and e - h Coulomb scattering in/between different LLs n (a) and subbands s (b), calculated for one-sided doped 20 nm GaAs quantum well at magnetic field $B = 15$ T.

for two GaAs quantum wells of different widths, both doped on one side to the same electron concentration $\rho = 2 \cdot 10^{11} \text{ cm}^{-2}$. The charge separation due to an electric field inside the well is significant for the $w = 20$ nm well and negligible for $w = 10$ nm. This is also confirmed by the indicated squared e - h overlaps $|\langle \chi_e | \chi_h \rangle|^2$.

To include the finite quantum well width in Coulomb matrix elements, the bare potential $V(r)$ must be replaced by an effective in-plane potential containing the appropriate form factors,

$$V_{s'_1, s'_2}^{s_1, s_2}(r) = \frac{e^2}{\epsilon} \int dz_1 dz_2 \frac{\chi_{s'_1}^*(z_1) \chi_{s'_2}^*(z_2) \chi_{s_1}(z_1) \chi_{s_2}(z_2)}{\sqrt{r^2 + (z_1 - z_2)^2}}. \quad (23)$$

On a sphere, $V_{s'_1, s'_2}^{s_1, s_2}(\theta)$ is obtained from the above by replacing r with $2Rv$, exactly as in Eq. (11) for the ideal 2D layers. In the matrix element $\langle i'_1; i'_2 | V | i_1; i_2 \rangle$ the first integral in Eq. (12) is unchanged, and the modified potential $V(\theta)$ enters only the one-body pseudopotential \mathcal{V} , which is hence no longer given by Eq. (16). However, since $\chi_e \neq \chi_h$, different effective potentials V and pseudopotentials \mathcal{V} must be used for e - e and e - h interactions.

Not being able to calculate \mathcal{V} analytically, we are forced to compute the entire tables of these 3D integrals for each choice of subband wave functions χ and $2Q$,

$$\mathcal{V}_{s'_1, s'_2, n}^{s_1, s_2, n'}(m) = \langle n', m | V_{s'_1, s'_2}^{s_1, s_2}(\theta) | n, m \rangle. \quad (24)$$

The above pseudopotential describes inter-LL scattering of an electron or a hole by an artificial charge that is localized at the north pole within the 2D sphere and undergoes transition between the subband states s_1 and s'_1 along the normal direction. It also can be converted into $\mathcal{V}(\mu)$ for the plane via $\mu = m - Q$.

Several examples of $\mathcal{V}(\mu)$ are plotted in Fig. 2 to illustrate the dependence on subband and LL indices. Despite a significant charge separation apparent in Fig. 1(a), the corresponding e - e and e - h pseudopotentials are rather

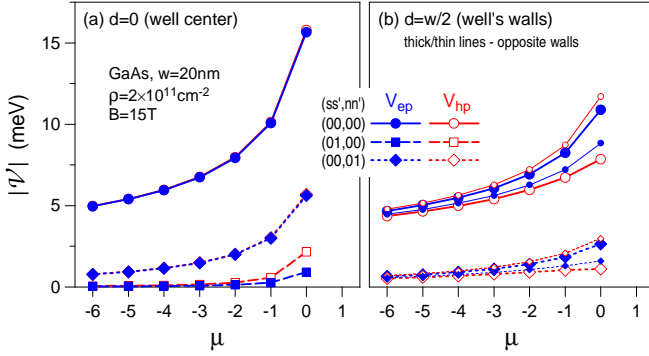


FIG. 3: (color online) Pseudopotentials similar to Fig. 2, but defined by Eq. (25) and describing interaction of an electron e^- or a hole h^+ with a point charge p^\pm located in the center (a) or at either wall (b) of the quantum well.

similar. However, the difference reaching almost 1 meV (for $w = 20$ nm, $\rho = 2 \cdot 10^{11} \text{ cm}^{-2}$, and $B = 15$ T) is sufficient to have a big effect on the trion binding energy.

Scattering by a point charge (ionized impurity) at a distance d from the middle of the well is described by a different pseudopotential,

$$\mathcal{V}_{s,n;d}^{s',n'}(m) = \langle n', m | V_{s,d}^{s'}(\theta) | n, m \rangle, \quad (25)$$

with the following effective potential,

$$V_{s,d}^{s'}(r) = \frac{e^2}{\epsilon} \int dz \frac{\chi_{s'}^*(z) \chi_s(z)}{\sqrt{r^2 + (z-d)^2}}, \quad (26)$$

where, as before, r is replaced by $2Rv$ for the sphere, and conversion to $\mathcal{V}(\mu)$ is immediate.

The examples in Fig. 3 illustrate the sensitivity to the impurity position d and to the electron or hole orbital indices s and n , as well as the electron/hole asymmetry. Remarkably, the energy scale of carrier-impurity interaction is not much (though nevertheless by up to 2 meV) greater than of the carrier-carrier interaction of Fig. 2.

The computation of a great number of needed integrals (24) can be accelerated by an adiabatic approximation in which the 3D integration is divided into the averaging of a squared relative z -coordinate

$$(\bar{D}_{s_1, s_2}^{s'_1, s'_2})^2 = \langle s'_1, s'_2 | (z_1 - z_2)^2 | s_1, s_2 \rangle, \quad (27)$$

and integration (only over θ) of an in-plane potential

$$\bar{V}_{s_1, s_2}^{s'_1, s'_2}(r) = \frac{e^2/\epsilon}{\sqrt{r^2 + (\bar{D}_{s_1, s_2}^{s'_1, s'_2})^2}}. \quad (28)$$

As its previous versions,^{31,51} the adiabatic approximation relies on \bar{D}^2 being small compared to $\langle n', m | r^2 | n, m \rangle$, so its accuracy depends on the in-plane quantum numbers. We found that, for a given combination of s 's and n 's, it is satisfactory for sufficiently small m . However, the

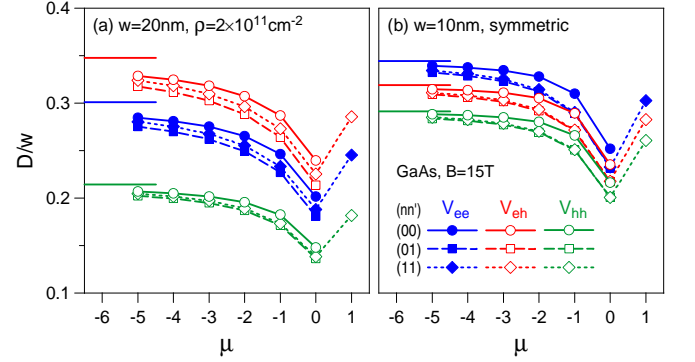


FIG. 4: (color online) Effective e - e , e - h , and h - h separations D in direction z normal to the quantum well plane defined by Eq. (29) as a function of relative angular momentum μ . Horizontal lines mark averages \bar{D} of Eq. (27). Different LL combinations (nn') are shown, for the lowest subband only. (a) Same system as in Fig. 2; (b) symmetric or undoped 10 nm quantum well. Magnetic field $B = 15$ T in both frames.

exact 3D integration must still be carried out for those several largest m 's (e.g., we chose $Q - m = -\mu \leq 5$).

A correct effective average separation D in the normal direction (such as to give the exact value of \mathcal{V}) can be defined for each set of s 's, n 's, and m by the requirement that (for this particular choice of quantum numbers)

$$\mathcal{V}_{s_1, s_2, n}^{s'_1, s'_2, n'}(m) = \langle n', m | \frac{e^2/\epsilon}{\sqrt{r^2 + (D_{s_1, s_2, n}^{s'_1, s'_2, n'})^2}} | n, m \rangle. \quad (29)$$

Certainly, $D_{s_1, s_2, n}^{s'_1, s'_2, n'} \approx \bar{D}_{s_1, s_2}^{s'_1, s'_2}$ for sufficiently small m , while it begins to depend on n' , n , and m as m increases and approaches Q (i.e., as $\mu = m - Q$ approaches zero). The typical dependences are shown in Fig. 4, with the averages of Eq. (27) also marked by horizontal lines. Evidently, D depends on n (or s , not shown) much less than \mathcal{V} does. On the other hand, using a constant value \bar{D} for all values of μ is not a justified approximation.

When the whole table of 3D integrals \mathcal{V} is known, the corresponding table of D 's can be immediately calculated by numerical solution of the 1D equations (29). We found that the values of $D(\mu)$ do not depend on the surface curvature nearly as much as $\mathcal{V}(\mu)$. Therefore, for a given quantum well (the width w and the set of subband wave functions χ) and magnetic field B , the time-consuming exact 3D integration of the \mathcal{V} table need only be performed for one value of $2Q$ and for several largest values of μ (e.g., we used $2Q = 20$ and $\mu \geq -5$). The approximate (but accurate) tables of \mathcal{V} for other values of $2Q$ are then quickly recovered from the corresponding table D , quickly computed from either Eq. (27) or (29), depending on μ . Finally, the two-body Coulomb matrix is calculated (analytically) from the coefficients \mathcal{V} in the same way as shown in Sec. II B 3 b for the ideal 2D layer.

C. Exact diagonalization

The hamiltonian matrices H were diagonalized numerically using a Lanczos based algorithm. The matrix was stored in a packed “compressed-row” format and divided into a number of segments that could fit in computer’s memory. The segments were loaded one by one during the matrix-vector multiplication (the only operation performed on the matrix – once in each Lanczos iteration). Since the vanishing of a matrix element $\langle i', j'; k' | H | i, j; k \rangle$ depends only on the two basis states, the location of non-zero elements (the most time-consuming part) had to be only done once for all used combinations of w , ϱ , or B .

To resolve all quantum numbers conserved by H and obtain the energy spectrum in the form of $E(S_z, S, L_z, L)$, the Lanczos procedure must be carried out inside the eigensubspaces of pair electron spin S (for the trion) and total angular momentum L (note that S_z and L_z are automatically resolved in the CI basis). The matrix elements of ladder operators $S^+ = \sum \sigma^+$ and $L^+ = \sum l^+$ (summations go over all particles) have a simple form in the CI basis, allowing analytic expression of the $\hat{L}^2 = L^+ L^- + L_z(L_z - 1)$ and $\hat{S}^2 = S^+ S^- + S_z(S_z - 1)$ matrices.

The initial Lanczos LS -eigenstates with desired eigenvalues of \hat{L}^2 and \hat{S}^2 were calculated using a conjugate-gradient method.⁵² To avoid dealing with two independent eigenproblems, we used a joint operator $\hat{S}^2 + 2\hat{L}^2$, whose eigenstates are simultaneous and unique eigenstates of both L and S (owing to their discrete spectra).

The accumulation of numerical errors leading to escape from the initially set LS subspace after more than a few Lanczos iterations was remedied by the LS -projection of each consecutive Lanczos state. When more than one lowest eigenstate was needed at some L and S , orthogonalization to all preceding Lanczos states was done at every iteration to avoid “ghost states.” Only three most recent Lanczos states were held in computer’s memory at the same time; all earlier ones were stored on a disk, in need of either the above-mentioned orthogonalization or recalculation of the eigenstates into the original CI basis.

Depending on spin and orbital symmetry, the diagonalization need not be repeated in every (S_z, S, L_z, L) subspace. In the absence of an impurity, it is only done for $L_z = 0$ (or $1/2$ if half-integral). Furthermore, the spin quantum numbers are only relevant for the trions, and their calculation was only carried out for $S_z = 0$.

III. CONVERGENCE AND ACCURACY

Being essentially a perturbative method, the CI exact diagonalization converges as a function of the size of the many-body CI matrix. Fast convergence requires that interactions are weak compared to the single-particle gaps. On the other hand, the maximum size of the CI matrix is limited by both the knowledge of low-energy single-particle spectra and by the computational capability.

TABLE I: Dimensions of the $2e + h$ configuration-interaction bases and corresponding numbers of above-diagonal non-zero matrix elements of the hamiltonian H , squared angular momentum \hat{L}^2 , and squared $2e$ spin \hat{S}^2 , for the $S_z = L_z = 0$ subspace and for different monopole strengths $2Q$ and maximum subband and LL indices s_{\max} and n_{\max} .

$2Q$	s_{\max}	n_{\max}	dimension	N_H	N_L	N_S
20	0	0	331	7620	2191	640
20	0	4	$0.6 \cdot 10^5$	$0.4 \cdot 10^8$	$0.4 \cdot 10^6$	$1.1 \cdot 10^5$
30	0	4	$1.1 \cdot 10^5$	$1.1 \cdot 10^8$	$0.8 \cdot 10^6$	$2.3 \cdot 10^5$
20	1	4	$4.6 \cdot 10^5$	$13.5 \cdot 10^8$	$3.1 \cdot 10^6$	$9.2 \cdot 10^5$
20	2	2	$2.9 \cdot 10^5$	$6.5 \cdot 10^8$	$1.9 \cdot 10^6$	$5.7 \cdot 10^5$

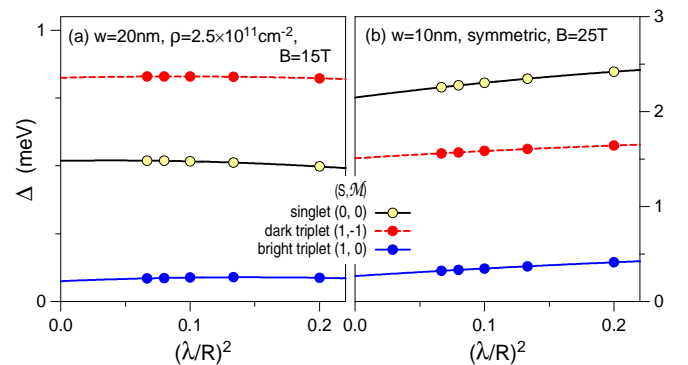


FIG. 5: (color online) Dependence of binding energies Δ of different trions X^- (distinguished by the $2e$ spin S and relative angular momentum M) on squared surface curvature (R is the sphere radius; λ is the magnetic length), calculated including five LLs and the lowest subband only for (a) one-sided doped 20 nm GaAs quantum well at magnetic field $B = 15$ T, and (b) symmetric/undoped 10 nm well at $B = 25$ T.

In Tab. I we list sizes of the H , L^2 , and S^2 matrices for several CI bases used in computation. The $2e + h$ hamiltonians are not very sparse ($2N_H/\dim > 1\%$), so numerical feasibility is defined almost exclusively by the number of their non-zero elements N_H (rather than by the space dimension or the sparsity of L^2 or S^2). For the largest basis we have used, compressed storage of a single H -matrix required over 15 GB of disk space.

Constrained by the manageable-size restriction and by limited knowledge of the matrix elements, we are still able to calculate some quantities with useful accuracy and to model various dependences at least qualitatively. Below we present several tests carried out to estimate convergence of our calculations of the trion binding energies Δ .

First, we analyze the finite-size and surface-curvature errors. In Fig. 5 we plot Δ calculated in two different systems (a narrow symmetric well in a high magnetic field and a wider asymmetric well in a lower magnetic field), including one subband and five LLs, as a function of the surface curvature $(\lambda/R)^2 = Q^{-1}$. The dependence is fairly weak, justifying the use of spherical geometry for the quantitative calculation. Moreover, the regular

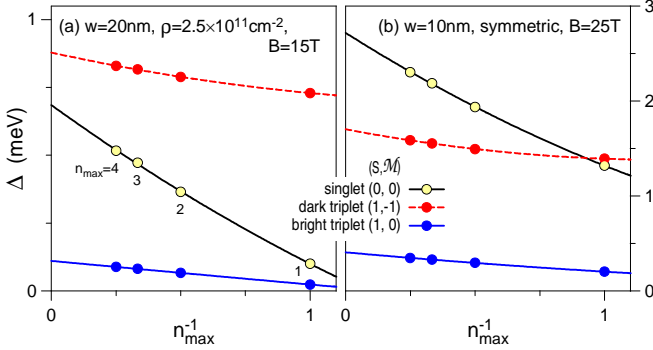


FIG. 6: (color online) Similar to Fig. 5 but with dependence on inverse maximum LL index n_{\max} (number of included LLs) calculated for $2Q = 20$ and including the lowest subband only.

behavior of $\Delta(Q^{-1})$ allows reliable extrapolation to the (planar) $R \rightarrow 0$ limit. In the following we used $2Q = 20$.

In Fig. 6 we study dependence on the number of included LLs. Although electron and hole cyclotron energies are different, we used the same maximum value n_{\max} for both particles, because the rotational symmetry of a sphere (or the magnetic translational symmetry of a plane) forbids mixing of different electron and hole LLs in the optically active ($k = 0$) exciton ground state: $\langle n'_e, m'_e; n'_h, m'_h | V | 0, m_e; 0, m_h \rangle \propto \delta_{n'_e n'_h}$. The dependence of Δ on n_{\max} is much stronger for the singlet trion than for both triplets. This is due to the stronger Coulomb interaction in this most compact state (the spin-unpolarized electrons have a large projection on the pair state with the minimum relative angular momentum $\mu = 0$, not allowed for in a triplet state), causing a more efficient mixing of different LLs. In the following we included five LLs ($n_{\max} = 4$). This promises to describe fairly accurately both triplet states, but Δ for the singlet state will probably be noticeably underestimated (by 0.2 and 0.4 meV in the two shown examples).

Inclusion of a great number of LLs is more difficult for the holes due to the complicated structure of the valence band. Since the correct energies ε_n of higher LLs are not known in general (for arbitrary w , ρ , and B), we largely ignore this complication by assuming equidistant LLs separated by the cyclotron energy taken from experiment for the lowest ($n = 0 \rightarrow 1$) transition. In Fig. 7 we test sensitivity of the results to this assumption by studying the dependence of Δ on the dimensionless factor ζ reducing the select (n th) hole's cyclotron gaps $\Delta\varepsilon_n = \varepsilon_{n+1} - \varepsilon_n$ compared to $\hbar\omega_c$ of Eq. (4). This test we have done for negative and positive trions, anticipating that the X^+ could show more dependence. The thin lines were obtained for all hole LLs spaced by the same $\Delta\varepsilon = \zeta\hbar\omega_c$. A more reasonable test is shown with the thicker lines, obtained for only the (unknown) gaps beyond the $n = 1$ LL being rescaled by ζ . The lack of strong dependence justifies the neglect of exact LL structure for the holes in the following calculation.

Finally, in Fig. 8 we analyze the effect of higher quan-

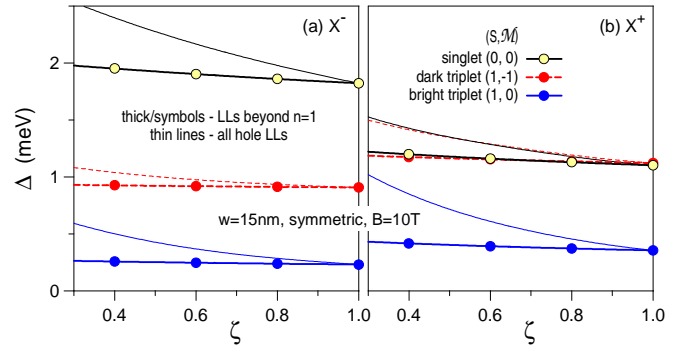


FIG. 7: (color online) Dependence of negative (a) and positive (b) trion binding energies Δ on factor ζ reducing the hole cyclotron gaps compared to Eq. (4), calculated for symmetric/undoped 15 nm quantum well at magnetic field $B = 10$ T, including five LL and two subbands. Thin lines: $\varepsilon_n = \varepsilon_0 + n\zeta\hbar\omega_c$ ($n \geq 1$); thick lines and symbols: $\varepsilon_1 = \varepsilon_0 + \hbar\omega_c$ and $\varepsilon_n = \varepsilon_1 + (n-1)\zeta\hbar\omega_c$ ($n \geq 2$), i.e., only higher gaps reduced.

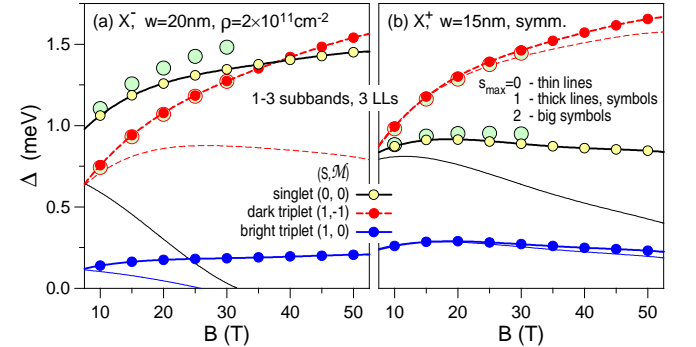


FIG. 8: (color online) Comparison of magnetic field dependences of negative and positive trion binding energies $\Delta(B)$ calculated including five LLs and between one and three subbands. (a) X^- in one-sided doped 20 nm GaAs quantum well; (b) X^+ in symmetric/undoped 15 nm well.

tum well subbands. On two examples (negative trions in a doped 20 nm well and positive trions in a symmetric 15 nm well) we compare the magnetic-field dependence of Δ calculated using three LLs and between one and two subbands. Analogously to the LL mixing, by far the strongest subband mixing occurs for the singlet trion. The effect is especially strong in both systems used here as the examples due the strong charge separation in the lowest subband for the X^- and having two heavy-mass particles in the X^+ . Evidently, the $s = 1$ subband must necessarily be included in the calculation for all trions in the presence of a doping layer, and at least for the singlet state in symmetric or undoped wells. However, the $s = 2$ and higher subbands can be neglected (except only for the singlet trions in wide asymmetric wells in high magnetic fields). Hence, two subbands ($s_{\max} = 1$) were included in the following calculations.

The results of this section can be summarized by two conclusions that we believe to be important in the com-

parison of numerical and experimental studies of trions. First, the dark and bright triplet states can be accurately modeled by exact diagonalization. The errors due to finite size, limited CI basis, or uncertainty in some microscopic parameters either do not affect these trions or can be eliminated (without need for extraordinary computer power). Second, numerical calculations for the singlet trion (by the CI exact diagonalization) are far more difficult due to a stronger sensitivity to the unknown sample-dependent parameters. However, note that even for the singlet X^+ we reached quite satisfactory agreement with the experiment of Vanhoucke *et al.* (cf. Fig. 3 of Ref. 28c).

A. Variational treatment of higher subbands

As a complementary account of the subband mixing we also used the following combination of exact diagonalization (in the plane of the well) and the variational approach (in the normal direction). The pair of model lowest-subband electron and hole wave functions

$$\chi(z) = \sqrt{2/w^*} \cos(z\pi/w^*), \quad (30)$$

where $w_e^* = w + 3.3$ nm and $w_h^* = w + 1.75$ nm denote the effective layer widths adequate for GaAs/Al_{0.35}Ga_{0.65}As symmetric wells and for $w = 10 - 30$ nm, were each rescaled by an arbitrary shrinking factor $\xi \leq 1$

$$\chi_\xi(z) = \xi^{-1/2} \chi(\xi^{-1} z). \quad (31)$$

The diagonalization was then carried out separately for the $e + h$ and $2e + h$ systems and for different combinations of electron and hole trial subband states χ_ξ . The result are the energy maps $E(\xi_e, \xi_h)$, separate for the exciton and each trion state. Having $\xi \neq 1$ costs single-particle energy, but stronger confinement imposed by $\xi < 1$ decreases total Coulomb energy of each bound state. The interpolation and minimization of E with respect to both variational parameters ξ yield, independently for the X and each X^- , the ground-state subband parameters $(\bar{\xi}_e, \bar{\xi}_h)$ and energies $E(\bar{\xi}_e, \bar{\xi}_h)$. The variational trion binding energies were calculated from Eq. (1) and, finally, the correction $\delta\Delta$ beyond the lowest-subband approximation was obtained by their comparison with the reference values obtained for $\xi_e = \xi_h = 1$.

In two frames of Fig. 9 we plot the calculated ξ_e and ξ_h as a function of w and B . The inaccuracy of the lowest-subband approximation, manifested by the interaction-induced distortion (squeeze) of the subband wave functions and measured by ξ , clearly increases as a function of both B and w . Both ξ_e and ξ_h are roughly linear in $(w/\lambda)^2 \propto w^2 B$. However, ξ_h is considerably smaller than $\xi_e \geq 0.98$ (which further enhances the $w_h^* < w_e^*$ asymmetry). Both ξ 's differ between the exciton and different trion states. Remarkably, ξ_h and ξ_e are anti-correlated in a sense that ξ_h decreases and ξ_e increases when going from X to X_{tb}^- , X_{td}^- , and X_s^- (at any given w and B).

The squeeze of subband wave functions shown in Fig. 9 confirms the main conclusions drawn from inclusion of

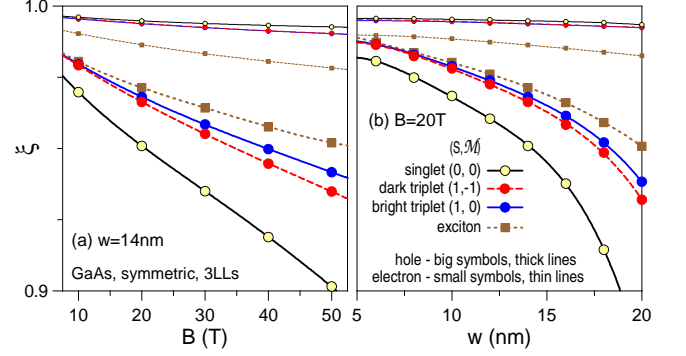


FIG. 9: (color online) Variational coefficients ξ of Eq. (31), rescaling widths of electron and hole wave functions compared to the noninteracting lowest-subband eigenstates, calculated for the exciton and trions in an undoped/symmetric GaAs well as a function of magnetic field B (a) and width w (b).

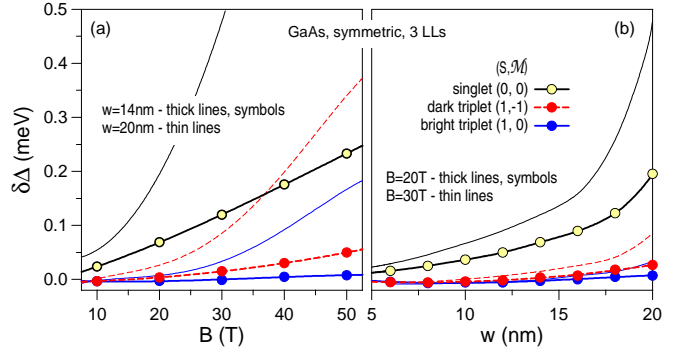


FIG. 10: (color online) Variational correction $\delta\Delta$ to the trion binding energies due to the squeeze of electron and hole wave functions compared to the noninteracting lowest-subband eigenstates, calculated for undoped/symmetric GaAs wells as a function of magnetic field B (a) and the well width w (b).

higher subbands directly into exact diagonalization (cf. Fig. 8). It predicts dependence on w and B , and explains why the subband mixing affects the singlet trion much more than both triplets. The variational correction $\delta\Delta$ beyond the lowest subband approximation are plotted in Fig. 10. Clearly, the quantitative agreement with exact diagonalization is rather poor (even if the comparison is made for the same $n_{\max} = 2$ restriction in each method). The reason is probably the combination of (i) the neglect of correlations in the normal direction within the variational calculation and (ii) the rather unrealistic choice of the trial subband wave function χ_ξ .

IV. RESULTS AND DISCUSSION

A. Exciton energy dispersion

Let us begin the discussion of trion binding energies Δ with an obvious observation that they strongly depend

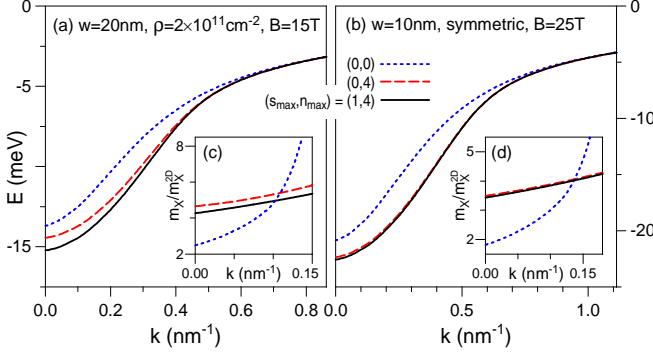


FIG. 11: (color online) Comparison of excitonic dispersions (energy E vs wave vector k) obtained with and without higher LLs and subbands, in different GaAs quantum wells. Insets: exciton Coulomb mass relative to the ideal value of Eq. (35).

on the energy spectrum of the exciton being captured by a free electron. This spectrum consists of a continuous in-plane dispersion $E(k)$ in each quantized subband.

In an ideal 2D system (lowest LL and zero width), exciton dispersion is known exactly,^{53,54}

$$E(k) = -\frac{e^2}{\lambda} \sqrt{\frac{\pi}{2}} e^{-\kappa^2} I_0(\kappa^2), \quad (32)$$

with $\kappa = k\lambda/2$ and I_0 being the modified Bessel function of the first kind. For small k ,

$$E(k) = -\frac{e^2}{\lambda} \sqrt{\frac{\pi}{2}} \left(1 - \kappa^2 + \frac{3}{4} \kappa^4 + \dots \right). \quad (33)$$

The curvature of $E(k)$ can be attributed to a “Coulomb mass” $m_X(k) = \hbar^2(\partial^2 E/\partial k^2)^{-1}$, which must not be confused with the single-particle electron or hole cyclotron masses. For an ideal 2D system, it follows from Eq. (32)

$$m_X(k) = \hbar^2 \left(\frac{e^2 \lambda}{2} \sqrt{\frac{\pi}{2}} \right)^{-1} \left(1 + \frac{9}{2} \kappa^2 + \dots \right). \quad (34)$$

At zero wave vector, the relation between $m_X \equiv m_X(0)$ and the interaction strength is particularly simple,

$$m_X = \frac{2\hbar^2}{\lambda^2 |E(0)|} \quad (35)$$

The magneto-exciton spectra in real quasi-2D structures were studied by Lozovik *et al.*,⁵⁵ so here we concentrate on the finite-width and LL/subband-mixing effects, illustrated in Fig. 11 for two different quantum wells at different magnetic fields. The ground state energy $E(0)$ which defines the maximum e - h attraction noticeably depends on both LL and (in the asymmetric well) subband mixing. In the insets we plot m_X divided by the value given by Eq. (35) for an ideal 2D system. In both quantum wells we find significant enhancement of m_X due to finite well width (by a factor ~ 2). Inclusion of higher LLs causes additional increase by another factor of ~ 2 , while the subband mixing has a much weaker effect.

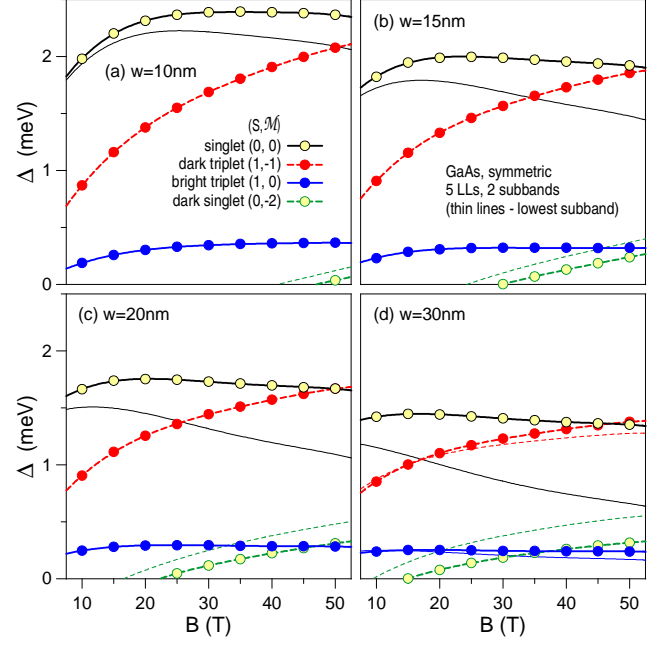


FIG. 12: (color online) Dependence of the trion binding energies Δ on magnetic field B , for undoped or symmetric GaAs quantum wells of different widths w . Different bound trion states are distinguished by the $2e$ spin S and relative angular momentum \mathcal{M} . Five LLs and up to two subbands were included in exact diagonalization on a sphere.

B. Trion binding energies

Let us now turn to the presentation of our main numerical results, that is to the dependence of the trion binding energies Δ in one-sided doped GaAs/Al_{0.35}Ga_{0.65}As quantum wells on w , ϱ , and B . The $\varrho = 0$ data are also adequate for the symmetrically doped wells. The calculations were carried out for $2Q = 20$ and including two subbands ($s_{\max} = 1$) and five LLs ($n_{\max} = 4$). The accuracy of this basis was discussed in Sec. III.

Plotted values of Δ are the Coulomb binding energies. The appropriate Zeeman terms must be additionally included to determine the absolute trion ground state or the energy splittings in the photoluminescence spectra.

Depending on the parameters, we found up to four different trions with significant binding energy in the energy spectra similar to Fig. 1 of Ref. 31. Besides the “singlet” X_s^- with $(S, \mathcal{M}) = (0, 0)$, “dark triplet” X_{td}^- (1,-1), “bright triplet” X_{tb}^- (1,0), an additional “dark singlet” X_{sd}^- (0,-2) was identified in some systems. Their binding energies will be denoted by Δ_s , Δ_{td} , Δ_{tb} , and Δ_{sd} .

In the following figures, the bright and dark states are distinguished by solid and dashed curves. On the other hand, the singlets and triplets are marked by open and full dots, respectively. The sets of curves obtained in the lowest-subband approximation (LSA) are also drawn for comparison with thin lines without the dots.

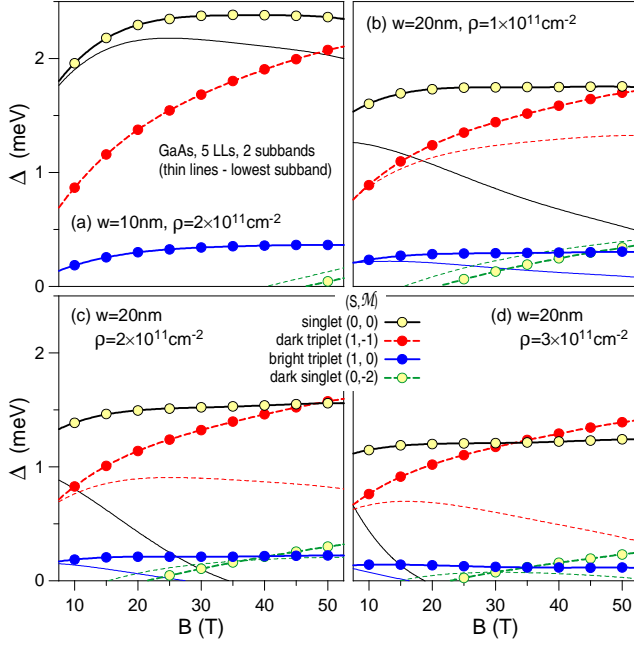


FIG. 13: (color online) Similar to Fig. 12, but for one-sided doped $w = 10$ and 20 nm GaAs quantum wells of different electron concentration ρ .

1. Dependence on magnetic field

We begin with the magnetic-field dependence shown in Fig. 12 for four symmetric quantum wells of different width and in Fig. 13 for two doped wells of different width and electron concentration. The singlet remains the most strongly bound state in all frames, with the singlet-triplet crossing pushed to much higher magnetic fields than anticipated by the earlier LSA calculations. Especially in the wide ($w = 20$ nm) doped wells the LSA fails completely, with the actual $\Delta_s(B)$ far more resembling that in the symmetric well. In all systems, $\Delta_s(B)$ and $\Delta_{tb}(B)$ rise at weak magnetic fields, but the increase saturates at $B = 15 - 30$ T (depending on w and ρ), beyond which both $\Delta_s(B)$ and $\Delta_{tb}(B)$ remain essentially flat at $\Delta_s = 1.5 - 2.4$ meV and $\Delta_{tb} = 0.2 - 0.4$ meV depending on w and ρ . In contrast, $\Delta_{td}(B)$ largely retains the characteristic \sqrt{B} dependence of an ideal 2D system ($w = 0$ and lowest LL). The weakly bound dark singlet emerges in wider wells and at higher fields, with a monotonically increasing $\Delta_{sd}(B)$.

2. Dependence on electron concentration

In Fig. 14 we study in more detail the dependence on electron concentration ρ . It was clear from Fig. 12 that the effect is negligible for narrow wells, so we only plot the data for $w = 20$ nm (with a relatively low $B = 10$ T and a very high $B = 40$ T compared in the two frames). Of all states, only the singlet shows a noticeable depen-

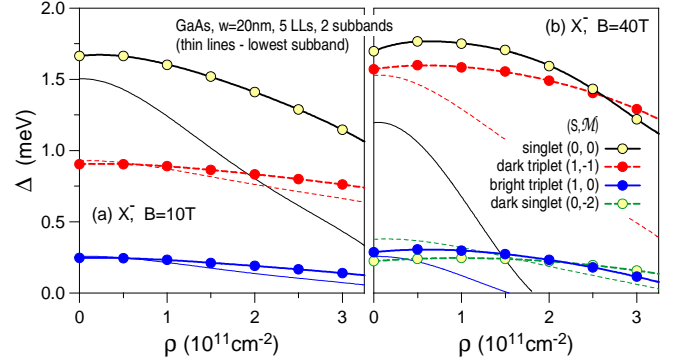


FIG. 14: (color online) Similar to Fig. 12, but with trion binding energies Δ plotted as a function of electron concentration ρ , for a 20 nm GaAs well at fields $B = 10$ T (a) and 40 T (b).

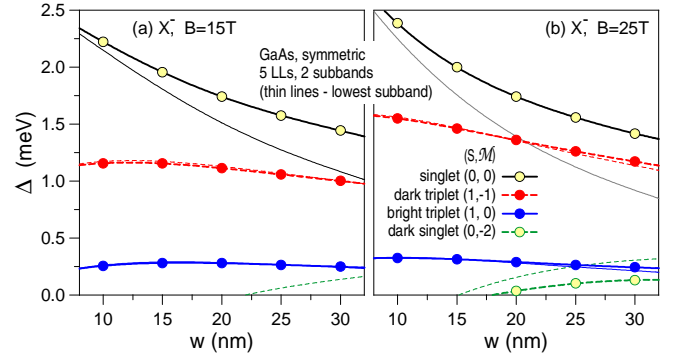


FIG. 15: (color online) Similar to Fig. 12, but with trion binding energies Δ plotted as a function of width w of a symmetric GaAs quantum well, at fields $B = 15$ T (a) and 25 T (b).

dence on ρ . However, it must be realized that if Δ were to be understood as the binding energy of a well defined bound state, at most weakly perturbed by the surrounding electrons, then B and ρ must be restricted to the values describing a sufficiently “dilute” system. A convenient measure is the LL filling factor $\nu = 2\pi\rho\lambda^2$ (proportional e.g. to the area of the dark triplet trion divided by the average area per electron). While for $B = 40$ T the system can be regarded dilute $\nu < 1/3$ throughout the frame, at $B = 10$ T the lowest LL fills completely ($\nu = 1$) already at $\rho = 2.4 \cdot 10^{11} \text{ cm}^{-2}$.

It is clear from Fig. 14 that the LSA fails completely to describe the effect of charge separation in asymmetric wells. It appears that, except for the extreme cases of highly doped wide wells, the effect can be simply ignored. However, if it need be included, the calculation must take into account the mixing with at least one higher subband.

3. Dependence on quantum well width

In Fig. 15 we plot Δ as a function of the width w (of a symmetric well) at two different magnetic fields. The LSA works remarkably well for the two triplet states,

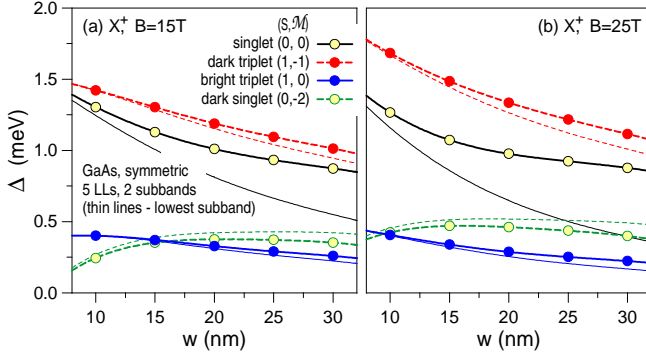


FIG. 16: (color online) Same as Fig. 15, but for positive trions.

neither of which shows a significant $\Delta(w)$ dependence throughout the wide range of $w = 10 - 30$ nm. In contrast, and in good agreement with the experiment of Vanhoucke *et al.* (cf. Fig. 5 of Ref. 28a), $\Delta_s(w)$ decreases markedly in the same range, although nearly not as much as predicted by the LSA.

In Fig. 16 we use the width dependence $\Delta(w)$ to illustrate the difference between negative and positive trions. Remarkably, at $B \geq 15$ T dark triplet is the most strongly bound X^+ throughout the entire shown width range $w = 10 - 30$ nm. Only the singlet positive trion has a lower binding energy than its negative counterpart. All other trions enhance their binding when going from X^- to X^+ . This is especially true of the dark singlet which emerges as an additional robust bound state in the X^+ spectrum. Also, the width dependence for the pair of triplets is more pronounced in the X^+ . Similarly as in X^- , the LSA works well for all positive trions except for the bright singlet.

4. Singlet-triplet crossing

From the comparison of binding energies of different trions one can try to establish the absolute trion ground state in a given quantum well (w and ρ) at a given field B . This might be especially important in the context of “quasiexcitons”,³⁷ proposed to form in incompressible electron fluids, such as the Laughlin fractional quantum Hall state at LL filling factor $\nu = 1/3$. Only those quasiexcitons formed from a dark triplet trion were found to cause discontinuity of the PL emission energy at $\nu = 1/3$, suggesting that an appropriate structure design (to achieve significant occupation of the dark triplet state) might be essential for optical detection of the Laughlin incompressibility.

In Fig. 17 we plot the critical magnetic field B_c at which the singlet-triplet crossing occurs in the trion Coulomb spectrum, as a function of both w and ρ . An accurate estimate of B_c is quite difficult due to accumulation of errors in the two compared Δ 's. Nonetheless, it is clear that inclusion of subband mixing favors the

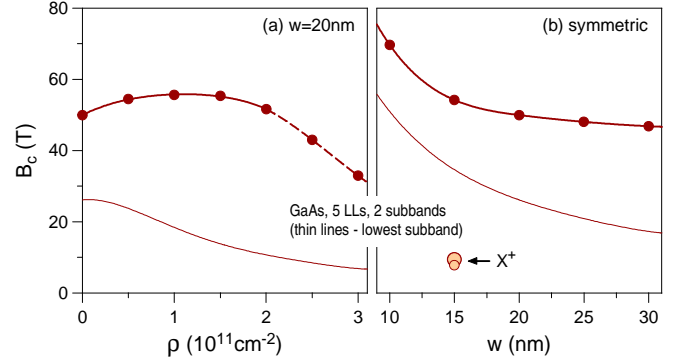


FIG. 17: (color online) Critical magnetic field B_c for the crossing of Coulomb binding energies of the singlet and dark-triplet states of the negative trion, as a function of electron concentration n (a) and quantum well width w (b). Open circles in (b) mark B_c for a positive trion in a $w = 15$ nm well.

singlet trion, pushing B_c to much higher values.

The fact that the LSA underestimates B_c was found by Whittaker and Shields³⁰ (for symmetric wells). It can be explained by the same perturbative argument we invoked earlier to explain different effect of the LL mixing on the singlet and triplet states: by noting that Coulomb interactions are stronger in the singlet state, causing more efficient mixing of excited single-particle states. However, in contrast to Whittaker and Shields, and in agreement with experiment of Vanhoucke *et al.* (cf. Figs. 5 and 6 of Ref. 28b), we find that B_c decreases as a function of w (e.g., leading to a crossing below 50 T in a 30 nm well).

Other conclusions from Fig. 17 are the following. Doping of even a fairly wide, 20 nm well has small effect on B_c up to $\rho \sim 2 \cdot 10^{11} \text{ cm}^{-2}$ (also, its decrease at higher concentrations is most certainly an artifact of the $s \leq 1$ approximation; cf. Fig. 8). The crossing of Coulomb binding energies calculated here is different from the crossing of the ground state energies due to additional electron Zeeman energy that must be added for the singlet (to lower B_c compared to our plot). It is also different from the crossing of recombination energies in the PL spectra, due to dependence of the hole Zeeman energy on a particular exciton or trion state.

In Fig. 17(b) we also marked B_c for a positive trion in a symmetric 15 nm well (small circle for LSA; large circle for $s \leq 1$). In good agreement with the experimental reports, it is much smaller than the value for X^- , predominantly due to the opposite effective-mass ratio.

5. Effect of nearby ionized impurities

Being charged, trions are efficiently localized by even fairly remote ionized impurities. Especially for the dark triplet, this might appear as a possible mechanism for breaking translational invariance of an otherwise perfect quantum well, needed for the explanation of experimentally observed optical recombination of this state. How-

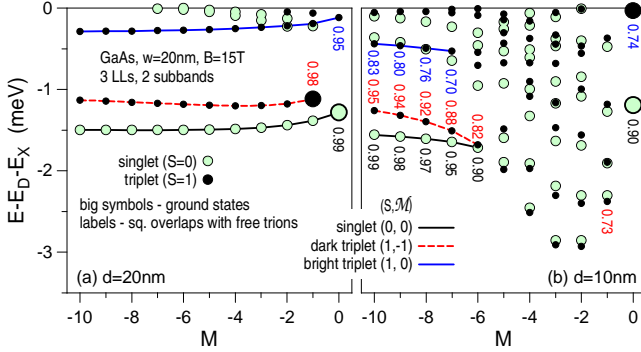


FIG. 18: (color online) Energy spectra of the $2e + h$ system in the presence of an ionized donor D^+ at a distance $d = w$ (a) and $d = w/2$ (b) from the well center (energy E , measured relative to an exciton unbound from the D^0 , plotted as a function of angular momentum on a plane M), calculated for a symmetric/undoped $w = 20$ nm GaAs quantum well at magnetic field $B = 15$ T, including three LLs and two subbands. Lines connect the D^+X^- states formed from different trions; the $S = 0$ and 1 ground states are marked with bigger symbols; and the color labels indicate squared overlaps with the corresponding free-trion states $|\langle X^- | D^+ X^- \rangle|^2$.

ever, Dzyubenko *et al.*⁵⁶ showed recently that this mechanism is not efficient. The $D^+X_{td}^-$ state was found stable only at sufficiently large distances d of the ionized donor D^+ from the center of the quantum well, at which its oscillator strength remains small ($\sim 1\%$ of the X_s^-).

We repeated this calculation in our model, but chose a wider, $w = 20$ nm quantum well and a higher field $B = 15$ T, in anticipation of a stronger effect of subband mixing induced by an off-center ($d \neq 0$) point charge. In Fig. 18 we compare the $2e + h$ energy spectra in the presence of a D^+ at $d = w$ and $w/2$. On the horizontal axis is the total angular momentum converted to the plane, $M = L_z - Q$ (neither L nor M are conserved in the presence of D^+ , leaving L_z or M as the only good orbital quantum number). The energy $E(M)$ is measured relative to the configuration consisting of a ground state exciton unbound from a neutral donor state $D^0 = D^+ + e$. The plotted energy difference is hence the negative of

$$\Delta(M) = E_X + E_D(M) - E(M), \quad (36)$$

which is the trion binding energy in the presence of a D^+ , generalized from Eq. (1). The singlet and triplet ground

states (states with the lowest E) are also indicated.

The average trion-donor distance depends on both d and M . At sufficiently large distances of the donor from the well (in our example, at $d \geq w$), the trion is captured without a significant distortion of its wave function. The lowest state for each trion occurs at $M = \mathcal{M}$ (trion's relative angular momentum). Each trion's Δ is slightly decreased, but the dependence on d or M is weak in this regime. In contrast, when the donor approaches the well, new trions bind and mix with X_s^- , X_{td}^- , and X_{tb}^- . The effect disappears at large $|M|$, but it is also relatively weak at $M = 0$, because the additional trions have $\mathcal{M} \neq 0$.⁵⁶ As pointed out in Ref. 56, for $d = w/2$ (donor at the wall of the quantum well), $\Delta = 1.2$ meV of the singlet ground state is only slightly smaller than $\Delta = 1.55$ meV of a free X_s^- , but the triplet ground state essentially unbinds.

V. CONCLUSION

We used exact numerical diagonalization on a sphere to calculate the energy spectra of negative and positive trions in doped GaAs quantum wells in high magnetic fields. The results obtained with the inclusion of up to three quantum well subbands were compared with a different method, combining exact diagonalization of the in-plane dynamics with a variational calculation for the normal direction. The obtained dependences of the trion binding energies Δ on the quantum well width w , electron concentration ρ , and magnetic field B significantly improve over previous theoretical estimates. In particular, the symmetric-well and lowest-subband approximations are both invalidated for a wide class of realistic systems. Presented detailed analysis of the accuracy and convergence establishes the exact diagonalization on a sphere for future quantitative studies of excitonic complexes. For example, it can be used for the analysis of exciton and trion wave functions ($e-e$ and $e-h$ correlations, oscillator strengths, LL/subband projections, etc.) or more detailed studies of the interaction of excitonic complexes with ionized impurities and/or free carriers.

Acknowledgment

Work supported by grants DE-FG 02-97ER45657 of US DOE and N20210431/0771 of the Polish MNiSW.

¹ F. Bassani and G. P. Parravicini, *Electronic States and Optical Transitions in Solids* (Pergamon, New York, 1975).

² E. L. Ivchenko, *Optical Spectroscopy of Semiconductor Nanostructures* (Alpha Science Int. Ltd., Oxford, 2005).

³ P. Hawrylak and M. Potemski, Phys. Rev. B **56**, 12386 (1997).

⁴ D. Heiman, B. B. Goldberg, A. Pinczuk, C. W. Tu, A. C. Gossard, and J. H. English, Phys. Rev. Lett. **61**, 605

(1988); B. B. Goldberg, D. Heiman, A. Pinczuk, L. N. Pfeiffer, and K. West, *ibid.* **65**, 641 (1990).

⁵ M. A. Lampert, Phys. Rev. Lett. **1**, 450 (1958).

⁶ K. Kheng, R. T. Cox, Y. Merle d'Aubigne, F. Bassani, K. Saminadayar, and S. Tatarenko, Phys. Rev. Lett. **71**, 1752 (1993).

⁷ F. M. Peeters, C. Riva, and K. Varga, Physica B **300**, 139 (2001).

- ⁸ I. Bar-Joseph, *Semicond. Sci. Technol.* **20**, R29 (2005).
- ⁹ A. Wójs and J. J. Quinn, *Proc. of 15th Int. Conf. on High Magnetic Fields in Semicond. Physics*, A. R. Long and J. H. Davies (Eds.), IOP Conference Series **171**, IOP Publishing, Bristol (2003); preprint: cond-mat/0308411.
- ¹⁰ B. Stebe and A. Ainane, *Superlatt. Microstruct.* **5**, 545 (1989).
- ¹¹ H. Buhmann, L. Mansouri, J. Wang, P. H. Beton, N. Mori, L. Eaves, M. Henini, and M. Potemski, *Phys. Rev. B* **51**, 7969 (1995).
- ¹² G. Finkelstein, H. Shtrikman, and I. Bar-Joseph, *Phys. Rev. Lett.* **74**, 976 (1995); *Phys. Rev. B* **53**, R1709 (1996).
- ¹³ A. J. Shields, M. Pepper, M. Y. Simmons, and D. A. Ritchie, *Phys. Rev. B* **52**, 7841 (1995).
- ¹⁴ D. Gekhtman, E. Cohen, A. Ron, and L. N. Pfeiffer, *Phys. Rev. B* **54**, 10320 (1996).
- ¹⁵ G. V. Astakhov, D. R. Yakovlev, V. P. Kochereshko, W. Ossau, J. Nürnberger, W. Faschinger, and G. Landwehr, *Phys. Rev. B* **60**, R8485 (1999); G. V. Astakhov, D. R. Yakovlev, V. P. Kochereshko, W. Ossau, W. Faschinger, J. Puls, F. Henneberger, S. A. Crooker, Q. McCulloch, D. Wolverson, N. A. Gippius, and A. Waag, *ibid.* **65**, 165335 (2002).
- ¹⁶ O. Homburg, K. Sebald, P. Michler, J. Gutowski, H. Wenisch, and D. Hommel, *Phys. Rev. B* **62**, 7413 (2000).
- ¹⁷ A. J. Shields, J. L. Osborne, M. Y. Simmons, M. Pepper, and D. A. Ritchie, *Phys. Rev. B* **52**, R5523 (1995).
- ¹⁸ S. Glasberg, G. Finkelstein, H. Shtrikman, and I. Bar-Joseph, *Phys. Rev. B* **59**, R10425 (1999).
- ¹⁹ I. V. Lerner and Yu. E. Lozovik, *Zh. Eksp. Teor. Fiz.* **80**, 1488 (1981) [*Sov. Phys. JETP* **53**, 763 (1981)].
- ²⁰ A. B. Dzyubenko and Yu. E. Lozovik, *Fiz. Tverd. Tela* **25**, 1519 (1983) [*Sov. Phys. Solid State* **25**, 874 (1983)].
- ²¹ A. H. MacDonald and E. H. Rezayi, *Phys. Rev. B* **42**, 3224 (1990).
- ²² A. Wójs and P. Hawrylak, *Phys. Rev. B* **51**, 10880 (1995).
- ²³ J. J. Palacios, D. Yoshioka, and A. H. MacDonald, *Phys. Rev. B* **54**, 2296 (1996).
- ²⁴ A. B. Dzyubenko and A. Y. Sivachenko, *Phys. Rev. Lett.* **84**, 4429 (2000); A. B. Dzyubenko, *Solid State Commun.* **113**, 683 (2000).
- ²⁵ M. Hayne, C. L. Jones, R. Bogaerts, C. Riva, A. Usher, F. M. Peeters, F. Herlach, V. V. Moshchalkov, and M. Henini, *Phys. Rev. B* **59**, 2927 (1999).
- ²⁶ F. M. Munteanu, Y. Kim, C. H. Perry, D. G. Rickel, J. A. Simmons, and J. L. Reno, *Phys. Rev. B* **61**, 4731 (2000); F. M. Munteanu, D. G. Rickel, C. H. Perry, Y. Kim, J. A. Simmons, and J. L. Reno, *ibid.* **62**, 16835 (2000).
- ²⁷ G. Yusa, H. Shtrikman, and I. Bar-Joseph, *Phys. Rev. Lett.* **87**, 216402 (2001).
- ²⁸ T. Vanhoucke, M. Hayne, V. V. Moshchalkov, and M. Henini, *Nanotechnology* **11**, 281 (2000); T. Vanhoucke, M. Hayne, M. Henini, and V. V. Moshchalkov, *Phys. Rev. B* **63**, 125331 (2001); *ibid.* **65**, 041307 (2002); *ibid.* **65**, 233305 (2002).
- ²⁹ C. Schüller, K.-B. Broocks, Ch. Heyn, and D. Heitmann, *Phys. Rev. B* **65**, 081301 (2002).
- ³⁰ D. M. Whittaker and A. J. Shields, *Phys. Rev. B* **56**, 15185 (1997).
- ³¹ A. Wójs, J. J. Quinn, and P. Hawrylak, *Phys. Rev. B* **62**, 4630 (2000).
- ³² A. Gładysiewicz, K. Wójcik, A. Wójs, and J. J. Quinn, *Acta Phys. Polon. A* **108**, 669 (2005).
- ³³ P. Redlinski and J. Kossut, *Solid State Commun.* **118**, 295 (2001); *Semicond. Sci. Technol.* **17**, 237 (2002); P. Redlinski, *J. Appl. Phys.* **99**, 063702 (2006).
- ³⁴ C. Riva, F. M. Peeters, and K. Varga, *Phys. Rev. B* **61**, 13873 (2000); *ibid.* **63**, 115302 (2001); *ibid.* **64**, 235301 (2001).
- ³⁵ G. V. Astakhov, D. R. Yakovlev, V. V. Rudenkov, P. C. M. Christianen, T. Barrick, S. A. Crooker, A. B. Dzyubenko, W. Ossau, J. C. Maan, G. Karczewski, and T. Wojtowicz, *Phys. Rev. B* **71**, 201312 (2005).
- ³⁶ D. Andronikov, V. Kochereshko, A. Platonov, T. Barrick, S. A. Crooker, and G. Karczewski, *Phys. Rev. B* **72**, 165339 (2005).
- ³⁷ A. Wójs, A. Gładysiewicz, and J. J. Quinn, *Phys. Rev. B* **73**, 235338 (2006).
- ³⁸ C. Schuller, K. B. Broocks, P. Schroter, C. Heyn, D. Heitmann, M. Bichler, W. Wegscheider, T. Chakraborty, and V. M. Apalkov, *Phys. Rev. Lett.* **91**, 116403 (2003).
- ³⁹ M. Byszewski, B. Chwalisz, D. K. Maude, M. L. Sadowski, M. Potemski, T. Saku, Y. Hirayama, S. Studenikin, D. G. Austing, A. S. Sachrajda, and P. Hawrylak, *Nature Physics* (London) **2**, 239 (2006).
- ⁴⁰ S. Takeyama, H. Kunimatsu, K. Uchida, N. Miura, G. Karczewski, J. Jaroszynski, T. Wojtowicz, and J. Kossut, *Physica B* **246**, 200 (1998); H. Kunimatsu, S. Takeyama, K. Uchida, N. Miura, G. Karczewski, T. Wojtowicz, and J. Kossut, *ibid.* **251**, 951 (1998); Y. Hirayama, K. Oto, H. Mino, K. Uchida, S. Takeyama, G. Karczewski, T. Wojtowicz, and J. Kossut, *Int. J. Mod. Phys. B* **18**, 3821 (2004).
- ⁴¹ L. Bryja, A. Wójs, and M. Potemski, *Phys. Rev. B* **73**, 241302(R) (2006).
- ⁴² F. D. M. Haldane, *Phys. Rev. Lett.* **51**, 605 (1983).
- ⁴³ T. T. Wu and C. N. Yang, *Nucl. Phys. B* **107**, 365 (1976).
- ⁴⁴ T. T. Wu and C. N. Yang, *Phys. Rev. D* **16**, 1018 (1977).
- ⁴⁵ J. J. Sakurai, *Modern Quantum Mechanics* (Addison-Wesley, Reading, 1994).
- ⁴⁶ J. E. Avron, I. W. Herbst, and B. Simon, *Ann. Phys. (N.Y.)* **114**, 431 (1978).
- ⁴⁷ B. E. Cole, J. M. Chamberlain, M. Henini, T. Cheng, W. Batty, A. Wittlin, J. A. A. J. Perenboom, A. Ardavan, A. Polisski, and J. Singleton, *Phys. Rev. B* **55**, 2503 (1997).
- ⁴⁸ I.-H. Tan, G. L. Snider, L. D. Chang, and E. L. Hu, *J. Appl. Phys.* **68**, 4071 (1990).
- ⁴⁹ W. Zawadzki and P. Pfeffer, *Semicond. Sci. Technol.* **19**, R1 (2004); P. Pfeffer and W. Zawadzki, *Phys. Rev. B* **72**, 035325 (2005).
- ⁵⁰ A. Gładysiewicz, L. Bryja, A. Wójs, and M. Potemski, *Phys. Rev. B* (in press).
- ⁵¹ J. R. Chapman, N. F. Johnson, and V. N. Nicopoulos, *Phys. Rev. B* **55**, R10221 (1997); *ibid.* **57**, 1762 (1998).
- ⁵² C. C. Paige and M. A. Saunders, *SIAM J. Numer. Anal.* **12**, 617 (1975).
- ⁵³ Yu. A. Bychkov, S. V. Iordanskii, and G. M. Eliashberg, *Pis'ma Zh. Eksp. Teor. Fiz.* **33**, 152 (1981) [*Sov. Phys.—JETP Lett.* **33**, 143 (1981)].
- ⁵⁴ C. Kallin and B. I. Halperin, *Phys. Rev. B* **30**, 5655 (1984).
- ⁵⁵ Y. E. Lozovik, I. V. Ovchinnikov, S. Y. Volkov, L. V. Butov, and D. S. Chemla, *Phys. Rev. B* **65**, 235304 (2002).
- ⁵⁶ A. B. Dzyubenko, D. A. Cosma, T. D. Kelly II, A. R. Todd, and A. Yu. Sivachenko, *cond-mat/0605071*.